ELSEVIER

Earth and Planetary Science Letters 195 (2002) 1–16

EPSL

www.elsevier.com/locate/epsl

The relationship between Martian gravity and topography

Dan McKenzie [a,*], David N. Barnett [a], Dah-Ning Yuan [b]

[a] *Institute of Theoretical Geophysics, Bullard Laboratories of the Department of Earth Sciences, Cambridge University, Madingley Rd., Cambridge CB3 0EZ, UK*

[b] *Jet Propulsion Laboratory, California Institute of Technology, 4800 Oak Grove Drive, Pasadena, CA 91109, USA*

Received 2 July 2001; received in revised form 10 October 2001; accepted 10 October 2001

Abstract

The relationship between gravity and topography of various regions of Mars is used to estimate their effective elastic thicknesses T_e using direct measurements of line of sight velocity, rather than spherical harmonic coefficients. Estimates of T_e vary from 70 km for Tharsis, 29 km for Elysium, to 14.5 km for the southern hemisphere, and show that the thickness of the Martian lithosphere increases with age as the radioactive isotopes of K, Th, and U decay. A simple parameterised model of the convective thermal history is used to estimate the temperature structure of the lithosphere, and shows that the base of the elastic layer has a temperature of 300 ± 50°C, or similar to the value for terrestrial continents. In both cases the rheology is probably affected by the presence of water. The short wavelength behaviour of the gravity field allows the density of the rocks that form the topography to be estimated, and gives values of about 3.0 Mg/m^3 for Tharsis and Elysium. This value is substantially greater than that of 2.7 Mg/m^3 obtained for Earth, and is in agreement with estimates from SNC (Shergottites–Nahklites–Chassigny) meteorites of 3.3 Mg/m^3. The density of the topography of Valles Marineris is only 2.35 Mg/m^3, and suggests that ice may be present below the surface. In the heavily bombarded southern hemisphere, isostatic compensation occurs at wavelengths as short as 700 km, which requires the effective compensation depth to be no more than 10 km. The gravity field with wavelengths greater than 1500 km may be supported dynamically, by a plume rising beneath the Tharsis region. The difference in temperature between the solidus and the present areotherm is less than 250°C, so melt generation can occur in rising plumes.

Keywords: Mars; elastic properties; convection; lithosphere; melts

1. Introduction

Because so little seismic information is yet available from Venus, Mars and the Moon, analysis of their external gravity fields and their topography is at present the principal method available for studying their interior structure [1]. The surface topography of rocky planets and satellites is supported by elastic forces in their outer layers. Such support causes short wavelength topography to be isostatically uncompensated, with compensation increasing with increasing wavelength. The resulting gravity anomalies can be used to estimate the effective elastic thickness, T_e, which is controlled by the temperature within the outer parts of a planet at the time that the load is imposed, and therefore contains information about

* Corresponding author. Tel.: +44-1223-337197.
E-mail address: mckenzie@esc.cam.ac.uk (D. McKenzie).

0012-821X/02/$ – see front matter
PII: S0012-821X(01)00555-6

Table 1
Estimates of Martian lithospheric parameters

	Wavelength band used km	ρ_c Mg/m^3	T_e km	Age Ga	T_p °C	F mW/m^2	T_{el} °C
Tharsis	380–1600	2.99	70	0	1261	17.8	340
Tharsis	380–700	2.97 ± 0.04					
V. Marineris	380–900	2.35	53				
Elysium (MGS)	350–900	2.98	29	2.2	1304	35.4	270
Elysium (Viking)	700–1000	(2.98)	25	2.2	1304	35.4	220
South Pole (flat)	400–800	(2.97)	14.5	3.5	1336	49.9	
South Pole (spherical)	400–3000	(2.97)	12.4	3.5	1336	49.9	

T_{el} is the temperature at the base of the elastic layer, whose thickness is T_e. The values of the parameters estimated from the SNC meteorites are $\rho_m = 3.50$ Mg/m^3, $E = 1.44 \times 10^{11}$ Pa and $\sigma = 0.268$ (McKenzie and McSween, in preparation) and were used to estimate T_e. A crustal thickness t_c of 30 km was used, except for the South Pole, where a value of 10 km was used for the flat plate and 8 km for the spherical cap. The average density of the meteorites believed to come from the Martian crust is $\rho_c = 3.32$ Mg/m^3. The values of ρ_c shown in parentheses were assumed, not estimated. The age estimates are from Hillier et al. [29], and are very uncertain [24].

past and present heat flow. It also controls the gravity field and the topography that result from mantle convection, and hence T_e must be estimated before such observations can be used to study mantle dynamics.

The transfer function Z between the Fourier transform of the topography $\overline{h}$ and free air gravity $\Delta\overline{g}$ when both are small is defined by $\Delta\overline{g} = Z\overline{h}$. Expressions for Z for a flat plate and a spherical shell are given in the Appendix, and the values of the parameters used are listed in Table 1. Fig. 1 shows $Z(k)$ as a function of $1/\lambda$ for a plane layer and a spherical shell, and for two values of t_c. At short wavelengths no isostatic compensation occurs, the value of $Z(=2\pi G\rho_c)$ is constant and is controlled only by the density of the surface topography ρ_c. As the wavelength increases, isostatic compensation occurs as the plate is deflected. The shape of this part of the curve is controlled by T_e and also by the density contrast $\Delta\rho$ at the Moho, the crust–mantle boundary. This paper uses the approach that has previously been applied to Earth and Venus [2,3] to estimate $Z(k)$, with two important modifications: one to take account of the large amplitude of the Martian topography and the other the polar orbits of Mars Global Surveyor (MGS) and Viking 2.

The first attempts to estimate T_e for Mars used Viking data [4,5]. The only topography available was obtained from stereo images, and the gravity field was also poorly known. MGS has now provided excellent topographic measurements [6,7], and two independent groups [8,9] have used the MGS tracking data to estimate the spherical har-

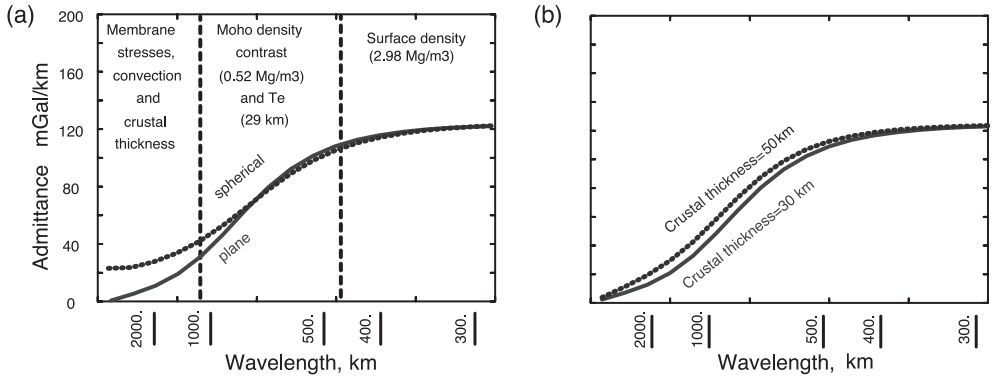

Fig. 1. Plot showing (a) the influence of sphericity, and (b) of crustal thickness on $Z(k)$.

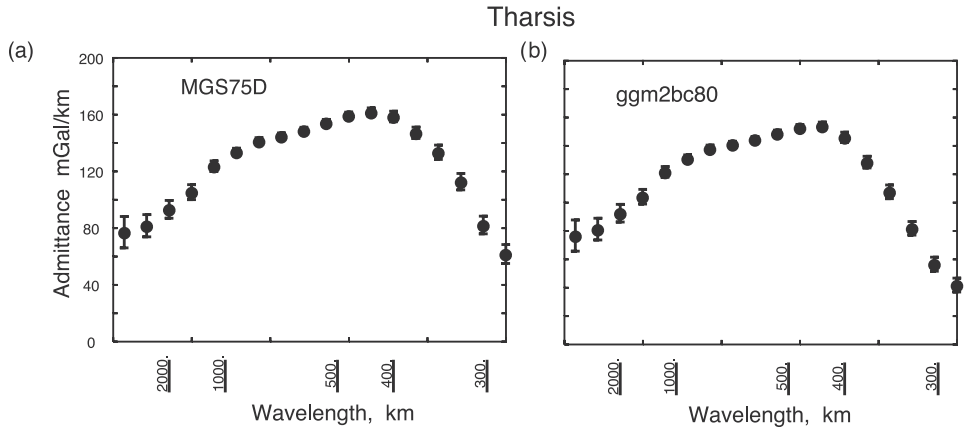

Fig. 2. Admittance calculated from the topography and (a) MGS75D gravity coefficients from JPL [8], and (b) ggm2bc80 gravity coefficients from Goddard space flight center [9], by projection onto a plane using Airy's projection [10] (see [2] for details).

monic coefficients of Mars's gravity and their results agree well. Therefore the standard approach to estimating T_e can now be used. Fig. 2a,b shows $Z(k)$ from both gravity fields for the Tharsis region (Fig. 3) of Mars, chosen because the amplitude of both the topography and gravity is large. The behaviour of $Z(k)$ differs in two important ways from similar estimates from Earth and Venus, and from the theoretical curves in Fig. 1. The short wavelength behaviour requires a value of ρ_c of about 3.4 Mg/m^3, in contrast to 2.7 Mg/m^3 for Venus and Earth, and the long wavelength behaviour is not well modelled by the deflection of an elastic plate. Such a value of ρ_c is greater than that of 3.32 Mg/m^3 calculated from the composition of the SNC meteorites (Table 1), which are generally accepted to be samples of Martian crust. Section 2 is largely concerned with these differences, and argues that the first partly results from the large amplitude of the topographic variations and partly from the large density of the surface topography, whereas the second results from the polar orbits of MGS and Viking 2 being viewed 'edge-on' during the periods when the best data were collected. The angles between the planes of the orbits and the line of sight (LOS) vectors to the Earth averaged $2.8 \pm 5.3°$ for MGS and $0.9 \pm 7.0°$ for Viking 2. Though some of the data used to determine MGS75D are from face-on orbits, their quality is not as good as those from the edge-on configuration. Once these effects are understood, it is straightforward to estimate T_e for other regions of Mars (Section 3). Estimates of the concentrations of U, Th and K based on compositions of the SNC meteorites are then used in Section 4 to estimate the temperature at the base of the elastic layer, using parameterised thermal history to estimate the surface heat flow, and hence the temperature structure within the lithosphere.

2. Data processing

We need to obtain the transfer function Z between topography $\overline{h}$ and gravity $\Delta\overline{g}$ over some region of Mars from the spacecraft observations in the frequency domain. The most obvious method of doing so is to use the spherical harmonic coefficients of the gravity field to calculate Δg, then to grid Δg and h in some projection that minimises the distortion. Standard Fourier methods can then be used to calculate Z (see [2] for details). The estimates of Z for Tharsis in Fig. 2a,b were obtained in this way. Although the two independent estimates closely resemble each other, there are two differences between both and the theoretical curves in Fig. 1. At wavelengths between 1000 and 450 km both are better represented by a straight line with positive slope than by a horizontal line. At longer wavelengths a straight line with a steeper slope fits the observed

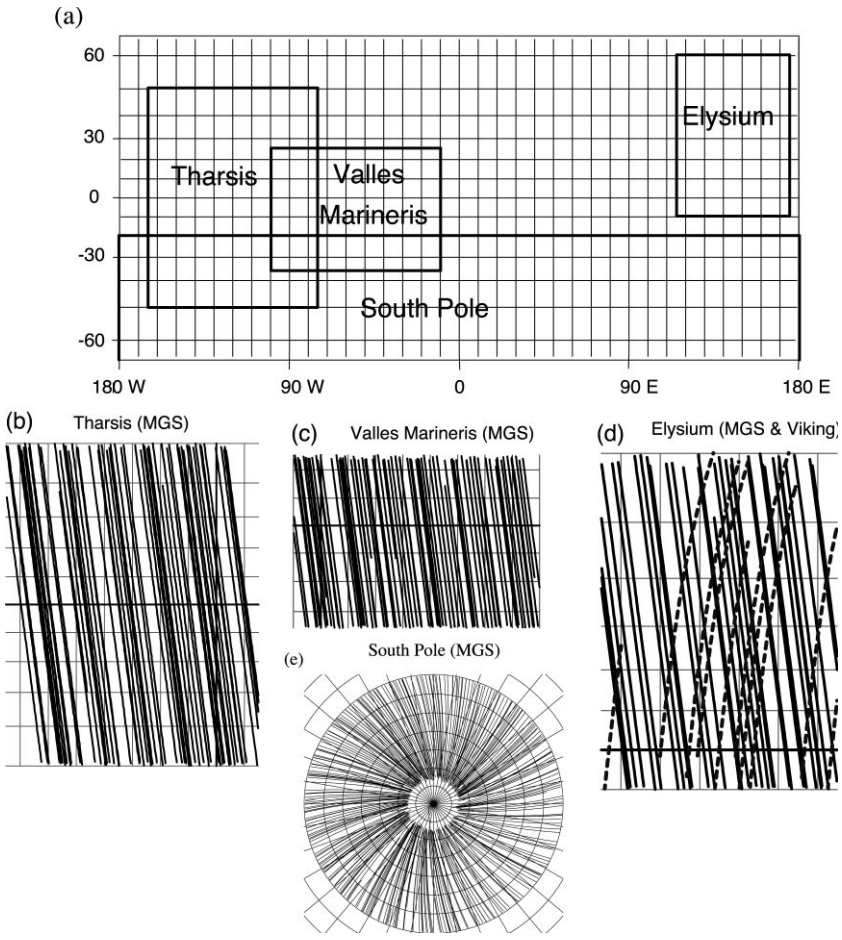

Fig. 3. Regions used to obtain the plots in Fig. 5. The solid lines show MGS tracks in b–e, and the dashed lines in d those of Viking 2.

estimates better than do the 'S'-shaped curves in Fig. 1.

One of these differences, the variation of Z at short wavelengths, results from an approximation. McGovern et al. [11] argue that the large amplitude of some of the topography on Mars causes the relationship between $\Delta\overline{g}$ and $\overline{h}$ to be nonlinear [12], and show that this problem becomes more important as the wavelength decreases. They take account of this effect by using the expressions relating topography to gravity on a spherical body obtained by Wieczorek and Phillips [13]. The second difference occurs at long wavelengths, where nonlinear effects are of minor importance. A likely explanation for this difference is that it results from the polar orbit of MGS (Fig. 3). The importance of using several spacecrafts with different heights and inclinations to determine the Earth's gravity coefficients is well known (see [14]). It is also well known that the effects of orbit resonance depend on a lumped combination of spherical harmonics [15]. It is therefore not surprising that the polar orbit used for MGS is not able to resolve the aliasing problem and determine the individual gravity coefficients accurately.

One solution to this problem is to use the tracking data to obtain $Z(k)$ directly, rather than from the harmonic coefficients of the gravity field. McKenzie and Nimmo [3] provide a method of doing so when the relationship between gravity

and topography is linear, and their approach can be extended to the nonlinear problem (there is a typographic error in their equation 8: the factor in front of the summation should be $1/a \sin\theta$ instead of $1/a$). The basic idea is to exploit the fact that the topography h of Mars is now well determined and therefore the spherical harmonic coefficients for h can be accurately calculated. It is then straightforward to extract that part of the acceleration of the spacecraft which is coherent with the topography. The algebra and programming is complicated because the true acceleration of the spacecraft is a vector, but only the component along the LOS from Mars to Earth can be observed and used to estimate Z. The relevant expressions are given in [3] and the Appendix.

Using these expressions, the calculated LOS acceleration can be obtained directly from the topography if Z is known. It is convenient to use a value of $Z = 1$ mGal/km in Eq. 5. With this choice:

$$\Delta\overline{g}_o = Z(\Delta\overline{g}_c + \overline{e}) + \overline{n} \quad (1)$$

gives Z in mGal/km, where $\Delta\overline{g}_o$, $\Delta\overline{g}_c$, $\overline{e}$, $\overline{n}$ are the Fourier transforms of the observed, Δg_o, and the calculated, Δg_c, LOS accelerations, of e, the error that arises from the neglect of the nonlinear contributions from Moho topography (see Appendix), and of n, the noise. The noise is defined as that part of the LOS acceleration that is incoherent with the topographic signal. Standard fast Fourier transform methods were used to obtain Z from Δg_o and Δg_c, with three tapers [16].

Most, but not quite all, values of the MGS Doppler velocities are provided as averages over 20 s, and over 10 s for Viking 2. Because the observed Doppler velocities are not all given at equal intervals in time, they were first linearly interpolated to give values every 20 s (MGS) and 10 s (Viking) before the LOS accelerations were calculated. Because the orbits of the spacecraft are not circular, the spacing of these positions along the tracks on the surface of the planet is not equal. The accelerations were therefore linearly interpolated onto points at intervals of 60 km (MGS) and 40 km (Viking) along the track before being Fourier transformed to obtain Z. The LOS Doppler data from both MGS and Viking supplied by JPL are the residual Doppler velocity, and are calculated with respect to orbits obtained from MGS75D. It was therefore necessary to add the LOS acceleration from MGS75D to the accelerations calculated from the residual Doppler velocities to obtain the full accelerations. The nonconservative accelerations were not restored to the Doppler residuals. The largest of these results from solar radiation pressure [6], and is accurately known. Its magnitude is ~ 0.01 mGal [6], or about an order of magnitude smaller than those of interest here. It does not correlate with the topography, and therefore does not affect the estimates of Z. The coherence between the LOS acceleration obtained from the residual Doppler velocity supplied by JPL and Δg_c, the LOS acceleration from the topography, is not significantly different from zero for either spacecraft. Hence there is in fact no useful information in the residual JPL Doppler. It is, however, important to recalculate the full accelerations, because the fitting process used to estimate T_e from the spectral observations uses their standard deviations, as well as their mean values.

Fig. 4a shows Z obtained directly from the MGS Doppler velocities. The observed values now vary with $1/\lambda$ in the way that is expected. Furthermore it is easy to show that it is the component of **g**(MGS75D) that is transverse to the tracks which causes the difference between Figs. 2 and 4a. The least well determined component of **g**(MGS75D) is in the plane that is normal to the LOS, and at right angles to the projection of the track in this plane (Fig. 4d). This component can be calculated from both MGS75D and the topography. The resulting values of Z are shown in Fig. 4b, and at long wavelengths are even larger than those in Fig. 2. The values of Z in Fig. 2 are averaged over all azimuths, and are therefore intermediate between those in Fig. 4a and b. Similar tests with similar results were carried out on the transverse components of **g** for the other boxes in Fig. 3. Fig. 4c shows the errors that arise from the neglect of the terms that are nonlinear in Moho topography. These are smaller

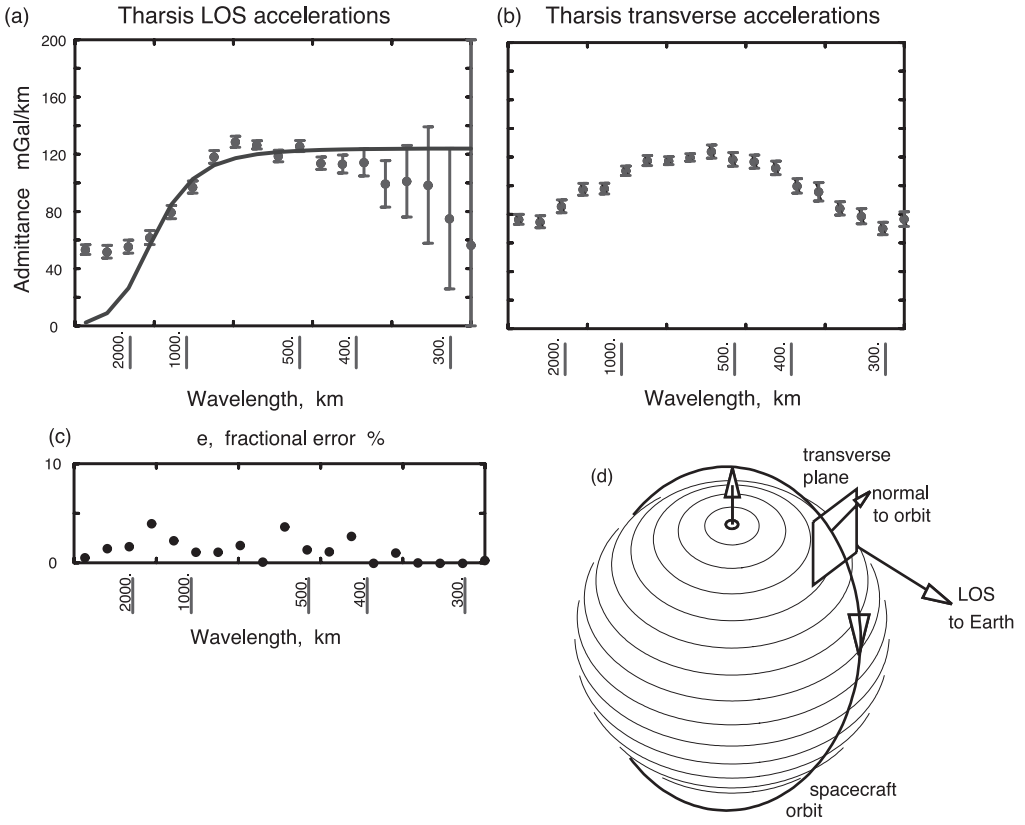

Fig. 4. Comparison of $Z(k)$, obtained from the LOS accelerations for the Tharsis box in Fig. 3b (a), with (b) those from topography and MGS75D calculated in the plane that is at right angles to the LOS vector, and normal to the orbit in this plane (d). The error caused by the neglect of the nonlinear terms in Moho topography is shown in c.

than the noise, and can anyway only be calculated if the Moho topography is known before the topographic load is emplaced. They can therefore be neglected.

Though the direct use of the Doppler velocities avoids using the poorly determined components of **g**, it does have one important disadvantage. Because it uses 1D transforms of the LOS accelerations along a number of tracks to calculate Z, rather than 2D transforms, there are fewer estimates of the complex amplitude in each wavenumber band. The 1D estimates of Z are therefore noisier than the 2D estimates, and larger regions are required to obtain accurate values. It is then more difficult to detect regional variations in T_e.

The final step in the data analysis consists of fitting a flexural model to the observed values of Z, $Z^i{}_o$, by minimising:

$$H \equiv H(T_e,\ \rho_c) = \left[\frac{1}{N}\sum_{i=1}^{N}\left(\frac{Z^i_o - Z^i_c}{\sigma_i}\right)^2\right]^{1/2} \qquad (2)$$

with respect to T_e and ρ_c, where $Z^i{}_c$ is calculated from the theoretical expressions given in [32] and the Appendix, and σ_i is the standard deviation of $Z^i{}_o$.

3. Observations

The methods explained in the last section are now used to estimate T_e and ρ_c for four regions of Mars shown in Fig. 3, and the values listed in Table 1. Our estimates of T_e are slightly smaller than those of McGovern et al. [11].

3.1. Tharsis region

The box in Fig. 3a labelled 'Tharsis' includes Olympus Mons as well as the three large volcanoes of Tharsis proper, and gives a crustal density of 2.97 ± 0.04 Mg/m^3. Though this value is substantially greater than the terrestrial value of 2.67 Mg/m^3, it is about 10% less than that obtained from the SNC meteorite compositions (Table 1). The difference probably results from porosity due to cracks and vesicles.

3.2. Valles Marineris

Fig. 5c shows that the short wavelength values of Z for Valles Marineris are smaller than those for Tharsis, and a value of ρ_c of 2.35 Mg/m^3 best fits the observed admittance. The best fitting value of T_e is also smaller than that for Tharsis. The low crustal density may be caused by a difference in composition between the Tharsis volcanoes and the walls of Valles Marineris. Another alternative is that the density is reduced by the presence of a large proportion of ice in the stratigraphic column. If the rock density is 3.32 Mg/m^3, the proportion of ice f required is 0.40 by volume, and could provide a source for the large amount of water required to account for the geomorphology of this region.

3.3. Elysium

Like Tharsis, this box also contains large volcanoes, but ones which are older than the Tharsis structures. The density agrees with that from Tharsis, but is less well determined, and T_e is smaller. The value of T_e from Viking 2 agrees reasonably well with that from MGS, but is likely to be less accurate, as it is based on fewer data of poorer quality (Fig. 3d).

3.4. South Pole

A large box (Fig. 3e) was required to obtain reliable estimates, principally because the values of Z are small for wavelengths larger than 600 km. Hence the decrease in Z that constrains the value of T_e occurs where the signal-to-noise ratio is small, and can only be determined if a large number of tracks are used. The surface of this part of Mars is old and heavily cratered. It is best fit by a small value of T_e of 14.5 km. Because T_e is small, the behaviour of Z at wavelengths of 500–800 km constrains the effective depth of compensation, which must be less than about 10 km to fit the observed values. The flat part of the theoretical curve $Z(k)$ occurs at wavelengths shorter than 250 km, where no reliable estimates of Z can be obtained because the data is noisy. Hence the data do not constrain ρ_c, and a value of 2.97 Mg/m^3 was used. Because of its elevation, it is unlikely that the average crustal thickness in the South Pole region is as small as 10 km. It is more likely that the crustal density is not constant, and that the density of the upper crust which forms the topography is lower than that of the lower crust and that of the large volcanoes.

3.5. Other data

All of the data discussed above come from Viking 2 and the Gravity Calibration Orbits of MGS between 5 February 1999 and 13 March 1999. An attempt was made to use data from the Science Phasing Orbits of MGS, but the resulting estimates of Z were not reliable.

3.6. Dynamic features and crustal thickness variations

Fig. 6 shows the long wavelength contributions to the topography, gravity and the areoid, the equipotential surface corresponding to the geoid on Earth, obtained by applying the filter in Fig. 6d directly to the spherical harmonic coefficients of the topography and MGS75D. The band pass filter is designed to remove shorter wavelength features that are elastically supported, and also those with the longest wavelengths. The contour levels for the gravity and topography are 50 mGal and 1000 m respectively, and therefore the maps should be identical if the admittance is everywhere 50 mGal/km.

The contour maps in Fig. 6a,b show that the large volcanoes of Tharsis, Alba Patera and Elysium have values of Z that are close to 50 mGal/

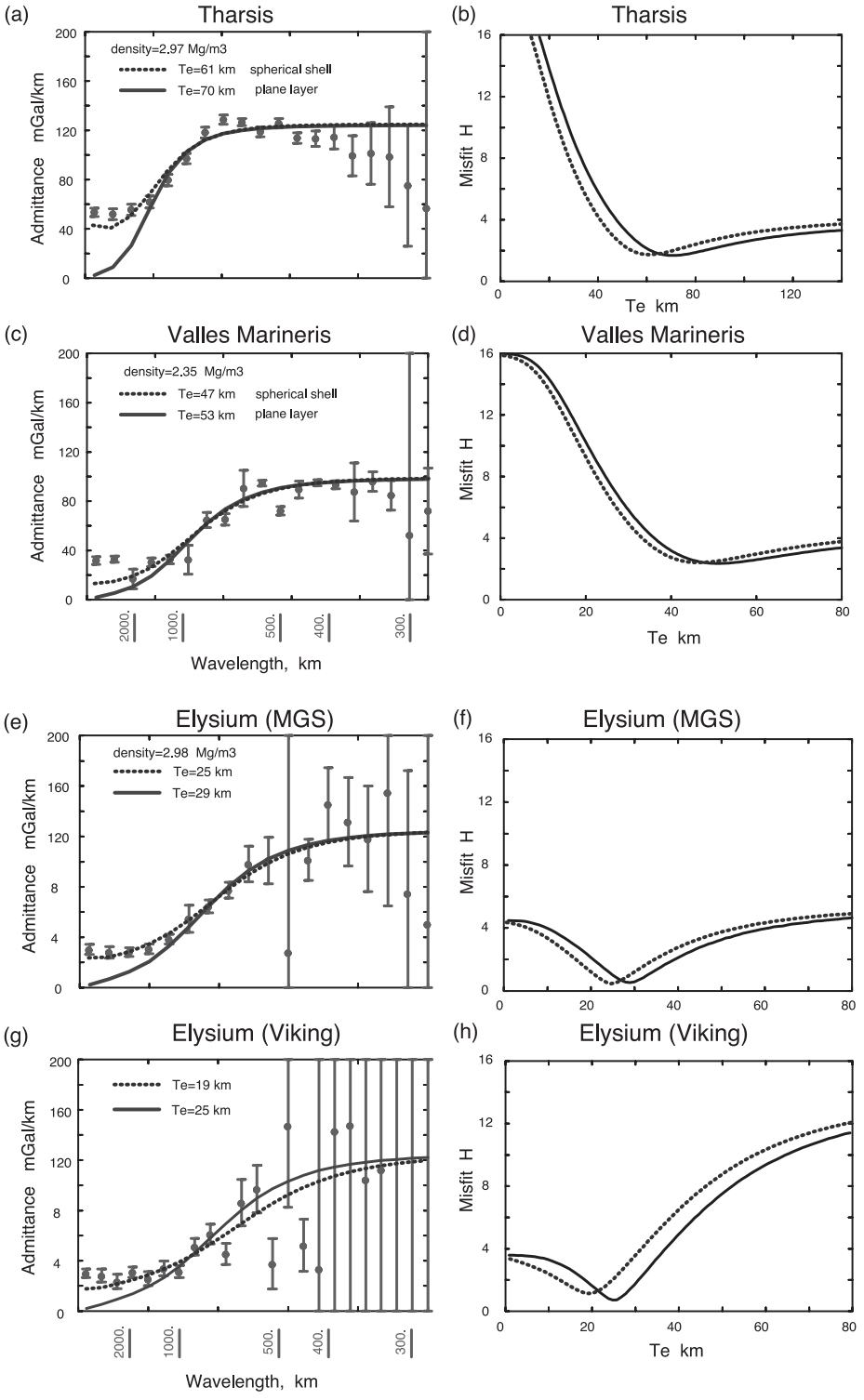
(a)
Tharsis
density=2.97 Mg/m3
Te=61 km spherical shell
Te=70 km plane layer
Admittance mGal/km
(b)
Tharsis
Misfit H
Te km
(c)
Valles Marineris
density=2.35 Mg/m3
Te=47 km spherical shell
Te=53 km plane layer
Admittance mGal/km
2000.
1000.
500.
400.
300.
Wavelength, km
(d)
Valles Marineris
Misfit H
Te km
(e)
Elysium (MGS)
density=2.98 Mg/m3
Te=25 km
Te=29 km
Admittance mGal/km
(f)
Elysium (MGS)
Misfit H
(g)
Elysium (Viking)
Te=19 km
Te=25 km
Admittance mGal/km
2000.
1000.
500.
400.
300.
Wavelength, km
(h)
Elysium (Viking)
Misfit H
Te km

Fig. 5.

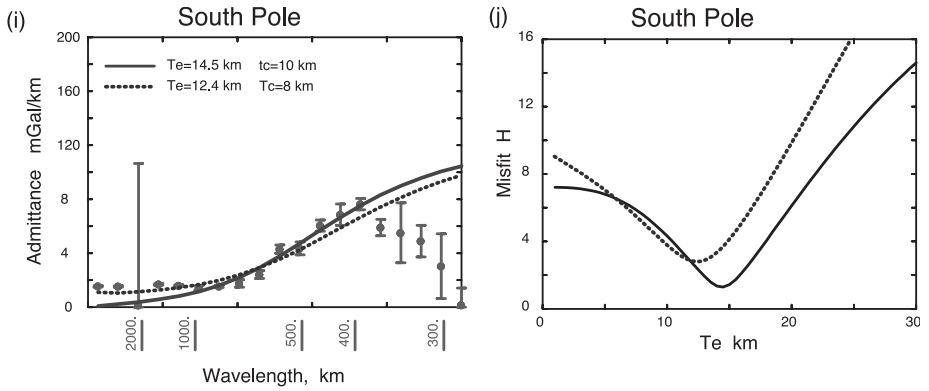

Fig. 5. Admittances and misfits H, calculated from Eq. 2, for the regions shown in Fig. 3, calculated from the LOS accelerations and the expected topographic accelerations along the MGS and Viking 2 tracks, shown in Fig. 3b–e. The continuous curves are those for a flat plate, those shown dotted are for a spherical shell.

km. The value of Z for Olympus Mons is, however, considerably larger than 50 mGal/km, and suggests that T_e for this volcano may be larger than 70 km. In agreement with Zuber et al. [1], Fig. 6a shows that the large impact basins of Argyre and Hellas both have small values of Z, and are therefore compensated by crustal thinning.

Long wavelength gravity anomalies with values of Z of 50 mGal/km or more must be supported dynamically, or by ring stresses if T_e is sufficiently large. The difference in behaviour between the plane and spherical models is caused by the presence of large ring stresses that arise in the spherical shell. For Tharsis Fig. 5a shows that the observed values of Z are 53.5 ± 2.4 mGal/km at wavelengths longer than 1500 km. Tharsis is the only region for which dynamic support may be required, and is only definitely necessary if the ring stresses are relaxed by dyke intrusion.

The areoid in Fig. 6c can be compared with Harder and Christensen's [17] calculated areoid for their 3D convective model. Their model of convection with volumetric heating rate H of 3.25×10^{-9} W/m^3 has one dominant plume after 4.5 Ga, and the height of their areoid is about 160 m after 7.8 Ga, compared with 700 m in Fig. 6c. Their heating rate is a factor of 3.6 less than the present day heating rate calculated from Wänke and Dreibus's [18] estimate of the abundances of U, Th and K if these elements are uniformly distributed throughout the Martian mantle. The difference between Harder and Christensen's calculated areoid and that observed may be caused by their estimate of H being too small or by the viscosity of the Martian mantle being greater than the value of 10^{21} Pa s that they use.

4. Thermal history

Temperature gradients within the lithospheres of convecting planets can only be estimated if the heat flux is known or if their thermal history can be calculated. On Earth the lower boundary of the continental seismogenic layer, the region of the continents that generates earthquakes, has a temperature of 350 ± 100°C [19], and has a thickness that is slightly greater than T_e. On Venus, however, the temperature at the base of the elastic layer is considerably greater, about 650°C [20], probably because both the crust and mantle of Venus are dry. For Earth, thermal history calculations are uncertain, because at least 70% of the present heat loss occurs by plate creation in the oceans, and nothing is known about the rates of oceanic plate production during most of its history. Mars and Venus, however, now have no plate boundaries whose separation rate is sufficiently fast to affect their heat budgets, so parameterised thermal history calculations for these planets [21,22] may be more reliable than they are for Earth. Mars is also small, and therefore has a shorter time constant than does either Venus or Earth. But three unresolved problems af-

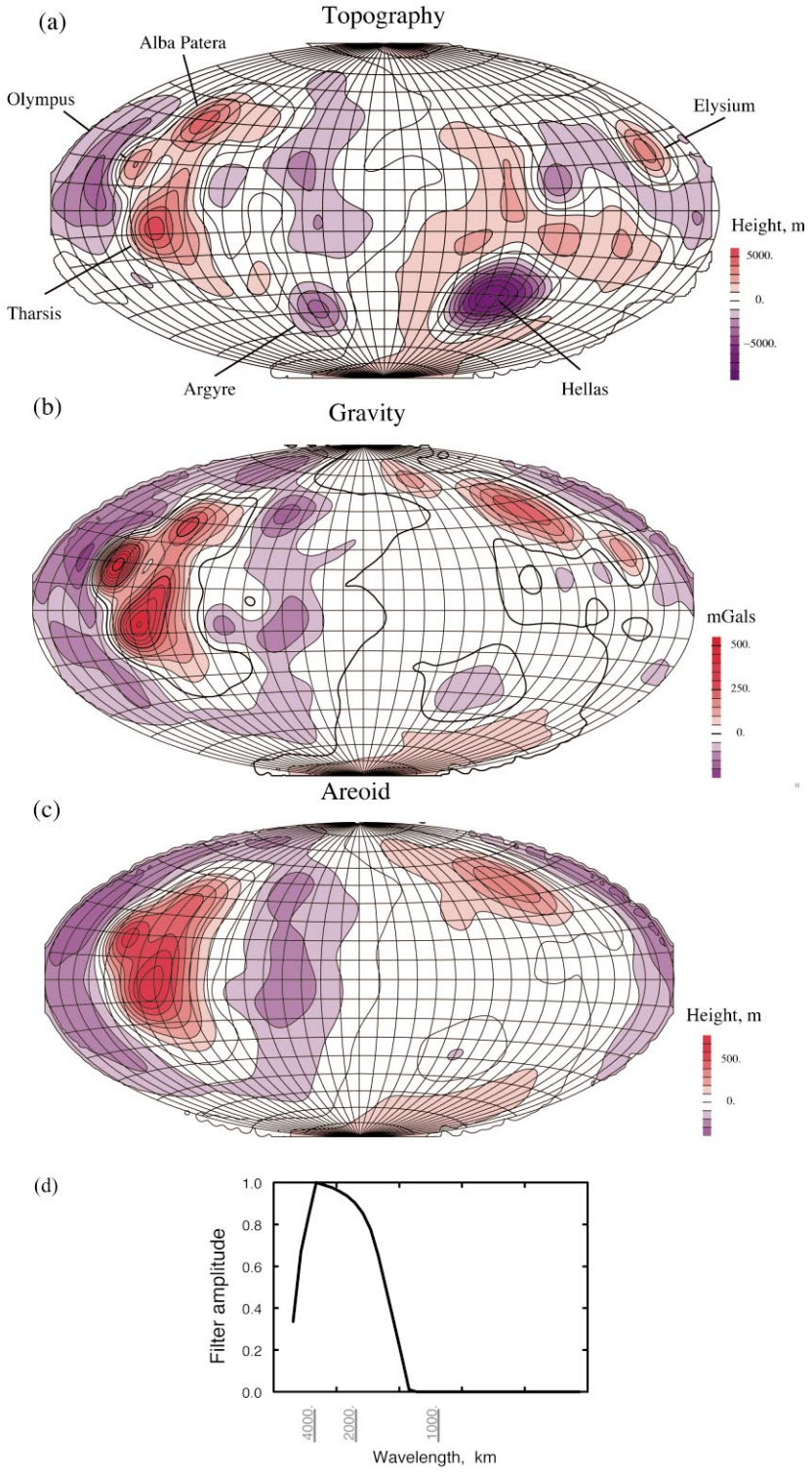

Fig. 6. Topography (a), gravity (b), and areoid (c) calculated from the spherical harmonic coefficients after low pass filtering using the filter in d.

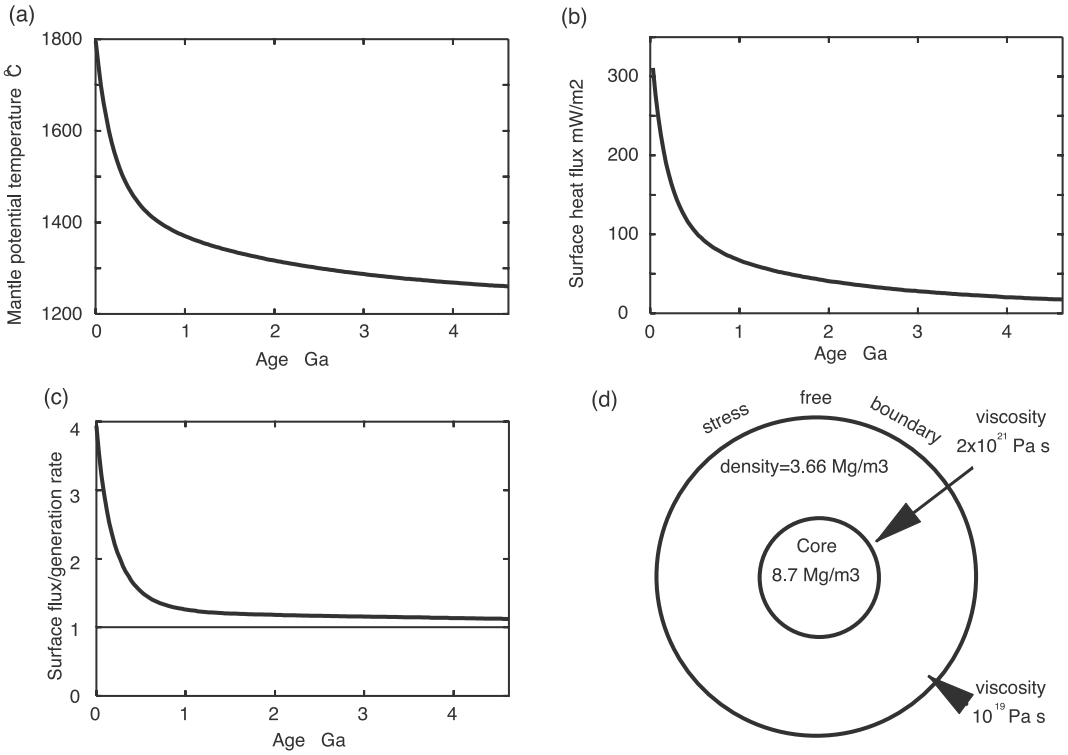

Fig. 7. Mantle potential temperature (a), heat flux (b) and heat loss/heat generation rate (c), for the spherical convective model shown in d, calculated using the expressions in [22] and the abundances of K, Th and U from [18].

fect such calculations. The first concerns elemental fractionation [23]. K, Th and U are among the most incompatible elements, and are removed from the source regions by melt fractions as small as 1%. Their concentrations in the Martian mantle therefore depend on the unknown extent to which Martian crust has been recycled early in Martian history. The second concerns estimates of the age of the Martian surfaces in the regions used to estimate T_e, which differ by more than 1 Ga [24]. Furthermore, the volcanoes must be older, and are perhaps much older, than the age of their surfaces. The last problem concerns the viscosity of the convective boundary layers which control heat transport. Their viscosity is as strongly affected by composition, and especially by the presence of water, as it is by temperature [25]. Until these problems are resolved it is not possible to carry out accurate convective thermal history calculations for Mars. We therefore used a simple two layer model of Mars (Fig. 7d) with a core of radius 1276 km [26] (Fig. 7d), and a mantle of constant composition [18]. Fig. 7a shows the evolution of the potential temperature of the mantle, obtained by analogy with Earth's old oceanic plates, by requiring the potential temperature to be 1300°C when the surface heat flux is 33.2 mW/m^2. Fig. 7c shows the ratio of the heat loss to the heat generation rate is 1.25 or less throughout the last 3.5 Ga of Martian history.

The thermal structure of the Martian lithosphere at various times (Fig. 8) was then calculated from the mantle potential temperature and the surface heat flux in Fig. 7 [27], using a viscosity of 10^{19} Pa s for the thermal boundary layer. Also shown in Fig. 8a,b are temperature profiles for potential temperatures that are 250°C hotter than those in Fig. 7a, similar to those of terrestrial plumes, but with the same thicknesses of the mechanical boundary layers. The temperature profiles in Fig. 8 show that such plumes can generate melt in the mantle below Martian litho-

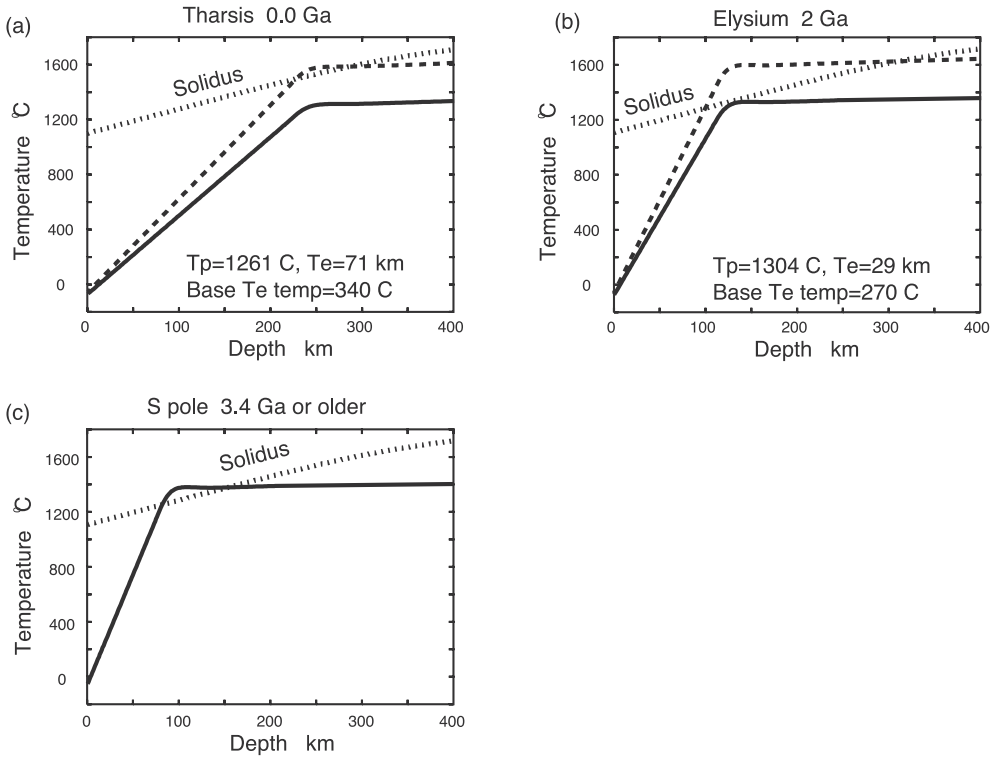

Fig. 8. Temperature as a function of depth within the Martian lithosphere at three epochs, calculated from the values of potential temperature and heat flux in Fig. 7a,b [27] and a surface temperature of −63°C. The solid curves are for the potential temperatures in Fig. 7a. The dashed curves show the effect of increasing these temperatures by 250°C without changing the lithospheric thickness.

sphere, and so produce the large volcanoes in the Tharsis and Elysium regions, some of which may still be active [28].

Fig. 8b also shows that the average temperature of the mantle below the lithosphere exceeds the solidus at ages greater than about 2.2 Ga, and therefore that the early thermal history of Mars cannot be modelled using this approach. Similar problems occur for Earth and Venus, because the rate of heat loss early in their history is controlled by different physical processes from those which now operate.

The temperature profiles in Fig. 8 can be used to estimate the temperature at the base of the elastic layer, and give values for Tharsis and Elysium of 340°C and 270°C respectively. These are similar to estimates of the temperature of the base of the seismogenic layer on Earth of 350 ± 100°C [19], but are considerably smaller than that for Venus, of about 650°C. The difference between the elastic properties of Venus and Earth is thought to result from the presence of a small amount of water in the Earth's mantle, and its absence within Venus [25]. The same effect can account for the low temperature at the base of the elastic layer on Mars if a small amount of water remains within the Martian mantle. Since considerable quantities of water have been present at the surface of Mars in the past, it is not surprising if some still remains in its interior.

5. Discussion and conclusions

Uncompensated topography with an amplitude of 1 km, a density of 3 Mg/m^3 and a wavelength of 400 km produces a surface gravity anomaly of amplitude 126 mGal. At a height of 400 km of the

MGS orbit the anomaly is reduced to 0.22 mGal. The corresponding variation in spacecraft velocity is 46 μm/s, and in height is 1 mm. These estimates show that accurate estimates of T_e for Mars are only possible because the velocity of MGS has been measured to an accuracy and precision of 100 μm/s or better using X-band telemetry. This remarkable data set allows the LOS acceleration to be calculated directly and compared with the topography. Though the Viking accelerations are from S-band tracking, and are therefore less accurate, the periapse height of 280 km is lower than that of 350–400 km of MGS. There is therefore less upward attenuation of the gravity anomalies in the Viking data. Because of the orbit and tracking geometry, a comparison between gravity and topography is better done using the LOS accelerations than by using surface gravity calculated from the spherical harmonic coefficients. In the frequency domain this comparison allows the elastic thickness T_e and density ρ_c of the surface topography to be estimated. Large volcanoes of the Tharsis region give a value of T_e of 70 km, whereas those of Elysium give a value of 29 km. The value of T_e for the old heavily cratered southern hemisphere is even smaller, 14.5 km. Estimates of ρ_c for Tharsis and Elysium are 2.97 and 2.98 Mg/m^3, or substantially greater than the value for Earth of 2.67 Mg/m^3. This difference is expected from the difference in composition between SNC meteorites and terrestrial basalts. The density of the topography of Valles Marineris is 2.35 Mg/m^3, and is smaller than that of the volcanoes, perhaps because of the presence of ice.

The variation of T_e with age of loading suggests that the Martian lithosphere has thickened as the planet has aged. Though the absolute ages of the regions are very uncertain, there is general agreement that the heavily cratered southern hemisphere is older than the Elysium volcanoes, which are in turn older than those of the Tharsis region [24]. Simple convective thermal history calculations suggest that the base of the elastic layer is controlled by the depth of the 300 ± 50°C isotherm. The critical temperature is therefore similar to the terrestrial value of 350 ± 100°C [19], presumably because a small amount of water is also present in the Martian mantle. The thermal structure of the Martian lithosphere and asthenosphere has been within 250°C of the solidus temperature throughout the last 2.2 Ga. Rising plumes whose potential temperature is 250°C greater than the average temperature of the upper mantle can therefore generate melt, even at the present day.

We were unable to estimate the crustal thickness, which only controls the relationship between gravity and topography at wavelengths where dynamic effects become important. Zuber et al. [1] obtained estimates by assuming that the crustal density is constant, but the crustal density difference of 0.6 Mg/m^3 between the Tharsis and Valles Marineris regions is larger than the density contrast of 0.5 Mg/m^3 between crust and mantle. Isostatic compensation in the southern hemisphere requires a density contrast at a depth of about 10 km. Unfortunately the orbit of the MGS spacecraft is too high to permit an estimate of the surface density ρ_c in this region, but it seems unlikely that the crust itself is as thin as 10 km. Variations of the thickness of a surface layer whose density is low, perhaps because it has been extensively fractured by impacts, seems a more likely explanation of the gravity observations.

Knowledge of the present day elastic thickness of the Martian lithosphere allows the gravity field to be low pass filtered, to remove features that are elastically supported. Maps of this long wavelength gravity and topography show that the Tharsis bulge may be supported dynamically.

Perhaps the most important result is that this study has led to few surprises. We now appear to understand, at least in outline, the processes that control the temperature structure of the lithospheres of Mars, Venus and Earth, support their topography by static and dynamic processes, and generate melt by mantle convection.

Acknowledgements

We would like to thank F. Nimmo, D. Stevenson, W. Sjogren, A. Konopliv, and H. McSween for their help, and M. Zuber for her thorough

review. This work was carried out while D.McK. was supported at the Division of Planetary Sciences, California Institute of Technology, by a Moore Fellowship. The research was also supported by the Natural Environment Research Council and by The Royal Society. Department of Earth Sciences contribution 6583. *[AH]*

Appendix

Wieczorek and Phillips [13] obtain an expression for the perturbation of the gravity potential ΔU produced by surface perturbations h to a spherical surface of mean radius R (= 3389.5 km) and Moho perturbations b to a surface of mean radius $R-t_c$, where t_c is the mean crustal thickness, in terms of ${}^n h'_{ilm}$ and ${}^n b'_{ilm}$ defined by:

$$h^n = R\sum_{ilm} {}^n h'_{ilm} Y_{ilm}(\theta,\ \phi),\ b^n =$$

$$(R-t_c)\sum_{ilm} {}^n b'_{ilm} Y_{ilm}(\theta,\ \phi) \qquad (3)$$

$Y_{ilm}(\theta,\ \phi)$ are spherical harmonics of degree l and order m normalised to 4π, with $Y_{1lm} = P_{lm}(\theta)\cos m\phi$, $Y_{2lm} = P_{lm}(\theta)\sin m\phi$, and $P_{lm}(\theta)$ are Legendre and Associated Legendre polynomials. We used values of n of 1–5. They show that the potential from a single deformed surface of mean radius R with density contrast $\Delta\rho$ is:

$$\Delta U = 2\pi G\sum_{ilm}\left(\frac{R}{r}\right)^{l+1} U'_{ilm} Y_{ilm}(\theta,\ \phi)$$

where:

$$U'_{ilm} = \frac{2R^2\Delta\rho}{2l+1}(h'_{ilm} + H'^{+}_{ilm})$$

G is the gravitational constant, and:

$$h'_{ilm} = {}^1 h'_{ilm},\ H'^{+}_{ilm} = \sum_{n=2}^{l+3}\frac{\prod_{j=1}^{n}(l+4-j)}{(l+3)n!}{}^n h'_{ilm} \qquad (4)$$

This notation is slightly different from [13] because the linear term has been separated from H'^{+}_{ilm}. We also need similar expressions for b'_{ilm} and B'^{+}_{ilm}, obtained by substituting b and B for h and H in Eq. 4. The spherical harmonic coefficients g_{ilm} of the perturbed gravity field Δg_c can then be written as:

$$\Delta g_c = \sum_{ilm} g_{ilm} Y_{ilm} \qquad (5)$$

where:

$$g_{ilm} = Z_l R(h'_{ilm} + H'^{+}_{ilm} + e'_{ilm})$$

$$Z_l = 2\pi G\rho_c A_l[1 + B_l/(1 + C_l/D_l)]$$

and:

$$e'_{ilm} = \frac{B_l(\rho_m-\rho_c)(h'_{ilm}B'^{+}_{ilm} + b'_{ilm}H'^{+}_{ilm})}{\rho_c h'_{ilm} + B_l(\rho_m-\rho_c)b'_{ilm}}$$

For a spherical shell:

$$A_l = (2l+2)/(2l+1),\ B_l = (1-t_c/R)^{l+3},$$

$$C_l = D[l^3(l+1)^3 - 4l^2(l+1)^2 +$$

$$8l(l+1)] + ET_e R^2[l(l+1)-2],$$

$$D_l = R^4 g(\rho_m-\rho_c)[l(l+1)-1+\sigma] \qquad (6)$$

[30,31], and for a flat sheet [32]:

$$A_l = 1,\ B_l = \exp(-kt_c),\ C_l/D_l = Dk^4/g(\rho_m-\rho_c) \qquad (7)$$

where $D = ET_e^3/12(1-\sigma^2)$, g is the mean acceleration due to gravity on the surface of the planet, ρ_c, ρ_m the crustal and mantle densities, E Young's modulus, σ Poisson's ratio, and k ($= (l+0.5)/R$) is the wavenumber. Z_l is the linear admittance between g_{ilm} and Rh'_{ilm}. The error e that results from assuming a linear relationship between g_{ilm} and $(h'_{ilm}+H'_{ilm})$ is therefore:

$$e = Re' = R\sum_{ilm} e'_{ilm} Y_{ilm} \qquad (8)$$

It contains terms that depend nonlinearly on the Moho deflection b and hence on T_e. In con-

trast, $h'_{ilm}+H'_{ilm}$ depends only on the surface shape, which is now well known, and only needs to be evaluated once. Therefore, if e is small, $Z(k)$ can be obtained directly from the calculated, Δg_c, and observed, Δg_o, LOS accelerations by Fourier transforming both series. Calculation of $Z(k)$ for any value of T_e then takes less than 0.1 ms. In contrast, the calculation of e' for one value of T_e takes about 5 h on the same machine, or a factor of about 2×10^8 longer. The average fractional errors $RZ(k)e'(k)/(\Delta g_c(k)+RZ(k)e'(k))$ for the Tharsis and Valles Marineris boxes with $T_e = 70$ km are 2% and 0.2% respectively, for Elysium with $T_e = 30$ km is 6%, and for the South Pole region with $T_e = 15$ km is 0.2%, for the wavelength bands given in Table 1 that were used to estimate T_e. These errors were calculated by evaluating the LOS acceleration resulting from Eq. (8) along the path of the spacecraft. Even the largest of these errors, for Elysium, is smaller than any of the uncertainties in $Z(k)$ in the relevant wavelength bands in Fig. 5e,g.

References

[1] M.T. Zuber, S.C. Solomon, R.J. Phillips, D.E. Smith, G.L. Tyler, O. Aharonson, G. Balmino, W.B. Banerdt, J.W. Head, C.L. Johnson, F.G. Lemoine, P.J. McGovern, G.A. Neumann, D.D. Rowlands, S. Zhong, Internal structure and early thermal evolution of Mars from Mars Global Surveyor topography and gravity, Science 287 (2000) 1788–1793.

[2] D. McKenzie, D. Fairhead, Estimates of the effective elastic thickness of the continental lithosphere from Bouguer and free air gravity anomalies, J. Geophys. Res. 102 (1997) 27,523–27,552.

[3] D. McKenzie, F. Nimmo, Elastic thickness estimates for Venus from line of sight accelerations, Icarus 130 (1997) 198–216.

[4] R.P. Comer, S.C. Solomon, J.W. Head, Mars: Thickness of the lithosphere from the tectonic response to volcanic loads, Rev. Geophys. 23 (1985) 61–92.

[5] W.B. Banerdt, M.P. Golombek, K.L. Tanaka, Stress and tectonics on Mars, in: H.H. Kieffer, B.M. Jakosky, C.W. Snyder, M.S. Matthews (Eds.), Mars, University of Arizona Press, Tucson, AZ, 1992, pp. 249–297.

[6] D.E. Smith, M.T. Zuber, S.C. Solomon, R.J. Phillips, J.W. Head, J.B. Garvin, W.B. Banerdt, D.O. Muhleman, G.H. Pettengill, G.A. Neumann, F.G. Lemoine, J.B. Abshire, O. Aharonson, C.D. Brown, S.A. Hauck, A.B. Ivanov, P.J. McGovern, H.J. Zwally, T.C. Duxbury, The global topography of Mars and implications for surface evolution, Science 284 (1999) 1495–1502.

[7] http://wufs.wustl.edu/geodata/mgscd/mola_egdr/ieg025_a.tab.

[8] G.L. Tyler, G. Balmino, D.P. Hinson, W.L. Sjogren, D.E. Smith, R. Woo, J.W. Armstrong, F.M. Flasar, R.A. Simpson, P. Priest, MGS RST Science Data Products, NASA Planetary Data System, MGS-M-RSS-5-SDP-V1.0 PDS label for Mars gravity model MGS75D, 2000. http://pds-geophys.wustl.edu/pds/mgs/rs/mors_1006/sha/jgm75d01.lbl.

[9] G.L. Tyler, G. Balmino, D.P. Hinson, W.L. Sjogren, D.E. Smith, R. Woo, J.W. Armstrong, F.M. Flasar, R.A. Simpson, P. Priest, MGS RST Science Data Products, NASA Planetary Data System, MGS-M-RSS-5-SDP-V1.0 PDS label for Mars gravity model GMM2B, 2000. http://pds-geophys.wustl.edu/pds/mgs/rs/mors_1008/sha/ggm2bc80.lbl.

[10] J.P. Snyder, An album of map projections, USGS Prof. Paper 1453, 1989.

[11] P.J. McGovern, S.C. Solomon, D.E. Smith, M.T. Zuber, G.A. Neumann, J.W. Head, R.J. Phillips, M. Simons, Gravity/topography admittances and lithospheric evolution on Mars: the importance of finite-amplitude topography, Lunar Planet. Sci. 32 (2001) 1804.pdf.

[12] R.L. Parker, The rapid calculation of potential anomalies, Geophys. J. R. Astron. Soc. 31 (1972) 447–455.

[13] M.A. Wieczorek, R.J. Phillips, Potential anomalies on a sphere: Applications to the thickness of lunar crust, J. Geophys. Res. 103 (1998) 1715–1724.

[14] F.G. Lemoine et al., The NASA and DMA joint geopotential model, EOS Trans. AGU 77 (Fall meet. Suppl.) (1996) F136.

[15] W.M. Kaula, Theory of Satellite Geodesy, Blaisdell, Waltham, MA, 1966.

[16] D.J. Thomsen, Spectrum estimation and harmonic analysis, Proc. IEEE 70 (1982) 1055–1096.

[17] H. Harder, U.R. Christensen, A one-plume model for Martian mantle convection, Nature 380 (1996) 507–509.

[18] H. Wänke, G. Dreibus, Chemical composition and accretion history of terrestrial planets, Phil. Trans. R. Soc. London Ser. A 235 (1988) 545–557.

[19] W.P. Chen, P. Molnar, Focal depths of intracontinental and intraplate earthquakes and their implications for the thermal and mechanical properties of the lithosphere, J. Geophys. Res. 88 (1995) 4183–4214.

[20] F. Nimmo, D. McKenzie, Volcanism and tectonics on Venus, Annu. Rev. Earth Planet. Sci. 26 (1998) 23–51.

[21] G. Schubert, S.C. Solomon, D.L. Turcotte, M.J. Drake, N.H. Sleep, Origin and thermal evolution of Mars, in: H.H. Kieffer, B.M. Jakosky, C.W. Snyder, M.S. Matthews (Eds.), Mars, University of Arizona Press, Tucson, AZ, 1992, pp. 147–183.

[22] F. Nimmo, D. McKenzie, Convective thermal evolution of the upper mantles of Earth and Venus, Geophys. Res. Lett. 24 (1997) 1539–1542.

[23] A. Weizman, D.J. Stevenson, D. Prialnik, M. Podolak, Modelling volcanism on Mars, Icarus 150 (2001) 195–205.
[24] R.G. Strom, S.K. Croft, N.G. Barlow, The Martian impact cratering record, in: H.H. Kieffer, B.M. Jakosky, C.W. Snyder, M.S. Matthews (Eds.), Mars, University of Arizona Press, Tucson, AZ, 1992, pp. 383–423.
[25] S.J. Mackwell, M.E. Zimmerman, D.L. Kohlstedt, High temperature deformation of dry diabase with application to the tectonics on Venus, J. Geophys. Res. 103 (1998) 975–984.
[26] C.M. Bertka, Y. Fei, Mineralogy of the Martin interior up too the core-mantle boundary pressures, J. Geophys. Res. 102 (1997) 5251–5264.
[27] D. McKenzie, M.J. Bickle, The volume and composition of melt generated by extension of the lithosphere, J. Petrol. 29 (1988) 625–679.
[28] W.K. Hartmann, M. Malin, A. McEwen, M. Carr, L. Soderblom, P. Thomas, E. Danielson, P. James, J. Veverka, Evidence for recent volcanism on Mars from crater counts, Nature 397 (1999) 586–589.
[29] K. Hillier, P. Janle, G.P.O. Neukum, J.E. Guest, R.M. Lopes, Mars: Stratigraphy and gravimetry of Olympus Mons and its aureole, J. Geophys. Res. 87 (1982) 9905–9915.
[30] D.L. Turcotte, R.J. Willeman, W.F. Haxby, J. Norberry, Role of membrane stresses in the support of planetary topography, J. Geophys. Res. 86 (1981) 3951–3959.
[31] R.J. Willemann, D.L. Turcotte, The role of lithospheric stress in the support of the Tharsis Rise, J. Geophys. Res. 87 (1982) 9793–9801.
[32] D.W. Forsyth, Subsurface loading and estimates of the flexural rigidity of the continental lithosphere, J. Geophys. Res. 90 (1985) 12,623–12,632.